# Expression of Calcium Channel Subunit Variants in Small Mesenteric Arteries of WKY and SHR

Robert H. Cox and Samantha Fromme

**BACKGROUND**
Enhanced function of dihydropyridine-sensitive $Ca^{2+}$ channels ($Ca_V$) in hypertensive arterial myocytes (HAM) is well accepted. Increased protein expression of pore forming $\alpha_1$-subunits contributes to this effect, but cannot explain all of the differences in $Ca_V$ properties in HAM. We hypothesized that differences in expression of $Ca_V$ subunits and/or their splice variants also contribute.

**METHODS**
RNA, protein, and myocytes were isolated from small mesenteric arteries (SMA) of 20-week-old male WKY and SHR and analyzed by polymerase chain reaction (PCR), sequencing, immunoblotting, and patch clamp methods.

**RESULTS**
Cav1.2 $\alpha_1$, $\beta_{2c}$, and $\alpha_2\delta_{1d}$ were the dominant subunits expressed in both WKY and SHR with a smaller amount of $\beta_{3a}$. Real-time PCR indicated that the mRNA abundance of $\beta_{3a}$ and $\alpha_2\delta_1$ but not total Cav1.2 $\alpha_1$ or $\beta_{2c}$ were significantly larger in SHR. Analysis of alternative splicing of Cav1.2 $\alpha_1$ showed no differences in abundance of mutually exclusive exons1b, 8, 21 and 32 or alternative exons33 and 45. However, inclusion of exon9* was higher and a 73 nucleotide (nt) deletion in exon15 (exon15Δ73) was lower in SHR. Immunoblot analysis showed higher protein levels of Cav1.2 $\alpha_1$ (1.61 ± 0.05), $\beta_3$ (1.80 ± 0.32), and $\alpha_2\delta_1$ (1.80 ± 0.24) but not $\beta_2$ in SHR.

**CONCLUSIONS**
The lower abundance of exon15Δ73 transcripts in SHR results in a larger fraction of total Cav1.2 mRNA coding for full-length $Ca_V$ protein, and the higher abundance of exon9* transcripts and $CaV\beta_{3a}$ protein likely contribute to differences in gating and kinetics of $Ca_V$ currents in SHR. Functional studies of $Ca^{2+}$ currents in native SMA myocytes and HEK cells transiently transfected with $Ca_V$ subunits support these conclusions.

*Keywords:* alternative splicing; blood pressure; $Ca^{2+}$ channel subunits; gene expression; hypertension; hypertensive rats; protein abundance; small mesenteric arteries; voltage gated $Ca^{2+}$ channels.

doi:10.1093/ajh/hpv024

Structural and functional remodeling of arteries is a universally accepted response to chronic hypertension.[1] This remodeling sustains and ultimately enhances hypertension leading to the well-described sequelae that contribute to the morbidity and mortality of this disease.[2] An important component of this remodeling is increased functional activity of dihydropyridine-sensitive, voltage-gated $Ca^{2+}$ channels ($Ca_V$).[3,4] Multiple mechanisms likely contribute to this effect including depolarized membrane potential and larger $Ca^{2+}$ currents with shifted voltage dependence of activation (about −5 mV) in arterial smooth muscle cells (ASMC).[5,6] Notably, differences have also been reported in $Ca^{2+}$ channel kinetics between normal and hypertensive ASMC.[7]

$Ca_V$ are multisubunit complexes composed of pore forming $\alpha_1$ along with accessory $\beta$ and $\alpha_2\delta$ subunits.[8] Multiple genes code for $Ca_V$ subunits many of which are subject to alternative splicing that significantly affect channel properties including antagonist sensitivity, gating, kinetics, and regulation.[8] The differences in gating and kinetics of $Ca_V$ cited above suggest that the enhanced activity in hypertension is not simply due to more of the same combination of $Ca_V$ subunits. Accordingly, this study was performed to test the hypothesis that differences in the expression profile of $Ca_V$ subunits and/or their splice variants contribute to the enhanced functional activity of $Ca_V$ in hypertensive ASMC.

## METHODS

### Animals and tissues

About 20–22 week-old male WKY and SHR (Charles River Labs., Wilmington MA) were used in these studies. Animal protocols were approved by the Lankenau Institute for Medical Research Animal Care and Use Committee. Studies were conducted in accordance with "The Guide for the Care and Use of Laboratory Animals."

Correspondence: Robert H. Cox (coxr@mlhs.org).

Initially submitted July 19, 2013; date of first revision August 28, 2014; accepted for publication February 3, 2015; online publication March 28, 2015.

**Program in Cardiovascular Disease, Lankenau Institute for Medical Research, Wynnewood, Pennsylvania.**

### RNA isolation and RT-PCR

ASMCs were dispersed from small mesenteric arteries (SMA) by papain and collagenase treatment from which total RNA was prepared using Tri reagent (RiboPure, Ambion; Austin, TX).[9] Total RNA was also prepared from the left ventricle free wall using Tri reagent, and from brain (WKY and SHR) by homogenization in guanidinium isothiocynate.[9] First-strand cDNA synthesis and conventional PCR (cPCR) were performed as described.[9]

### Quantitative PCR

Quantitative PCR (qPCR) was performed in triplicate using an Eppendorf ep *realplex* (Hamburg GR) with qTaq polymerase (Life Technologies; Grand Island, NY) and gene expression assays (Applied Biosystems; Foster City, CA and Operon Labs; Huntsville AL) as described.[9] The abundance of potential reference genes was compared in WKY and SHR. As expression of β-actin, Rsp5, and Tpt1 was similar (Supplementary Figure S1) the most abundant (β-actin) was used for normalization.

### Sequencing

To analyze exon content of transcripts, target sequences were amplified by PCR using Advantage HF2 polymerase (Clontech; Mountain View, CA), gel purified, A-tailed, cloned into a TOPO TA vector (pCR2.1, Life Technologies), and used to transform competent TOP10 cells (Life Technologies).[9,10] Colonies were selected, cultured overnight, used for plasmid DNA isolation (Qiagen Miniprep; Valencia, CA)[9,10] and sequenced on both strands at the Kimmel Cancer Center of Thomas Jefferson University.

### Colony PCR

Single colonies from plates prepared as above were used as template for PCR with primers that spanned multiple exons. PCR reactions were separated on agarose gels, stained with ethidium bromide, visualized with a MultiFluor S imager and analyzed by Quantity One software (Bio-Rad; Hercules, CA).[9,10]

### Protein analysis

Proteins were isolated from tissue by homogenization in RIPA buffer (Sigma Chemical, St. Louis, MO) with protease inhibitors (Complete mini, Roche Diagnostics; Indianapolis, IN) and analyzed by Western blot as described.[9,10]

### Transfections

Expression constructs for Cav1.2 $\alpha_1$, $\beta_2$, and $\alpha_2\delta_1$ in pcDNA3 were kindly provided by Dr Richard Swanson (Merck Research Laboratories; West Point, PA). A construct for Cavβ3 was generated by PCR from SMA RNA using Advantage HF2 polymerase (Clontech Laboratories; Mountain View, CA) and ligated into pcDNA3.1-Directional-V5/His-TOPO (ThermoFisher Scientific). All constructs were sequenced completely on both strands to confirm their accuracy. The Cav1.2 $\alpha_1$ construct used was similar to the smooth muscle variant that includes exons 1b, 8, 15 complete, 21, 32, and 33, but excludes exons 9* and 45.[11,12] HEK293 cells (ATCC; Manassas, VA) were transfected with the $Ca_V$ subunit (1:2:2 molar ratio) and pEGFP plasmids (Clontech) using FuGENE HD (Roche Diagnostics, Basel, Switzerland) and maintained in culture until used 48–72 hours later.

### Electrophysiology

HEK cells were placed in a chamber on an inverted microscope (Diaphot, Nikon Instruments; Melville, NY) and superfused with a solution containing (mmol/l) 140 NaCl, 5 KCl, 1 $MgCl_2$, 2 $CaCl_2$, 10 HEPES, and 10 glucose (pH 7.4 with NaOH). $Ca^{2+}$ currents ($I_{Ca}$) were recorded at room temperature (~21 °C) in the whole cell configuration using an Axopatch 200B amplifier controlled by pCLAMP 10.2 software (Molecular Devices, Sunnydale, CA). Micropipettes (WPI; Sarasota, FL) had resistances of 1.5–2.5 MΩ when filled with internal solution containing (in mmol/l) 100 CsCl, 20 TEACl, 5 NaCl, 1 MgCl, 5 $Na_2ATP$, 20 HEPES, 10 BAPTA 0.01 cAMP, and 0.1 NaGTP (pH 7.3 with CsOH). Pipette offset and stray capacitance as well as whole cell capacitance and series resistance were compensated optimally, and series resistance prediction and correction were adjusted to 85% or higher. Voltage and current data were recorded on a computer for offline analysis using Clampfit 10.2 and SigmaPlot 12.0 (Systat, Chicago, IL) software.

### Statistics

Statistical analyses were performed with SigmaPlot v12.0 (Systat Software, San Jose, CA). Values of $2^{-\Delta\Delta C_t}$ from real-time PCR analysis (Figures 1 and 2) and $Ca_V$ subunit protein abundance (Figure 4) for SHR/WKY were tested for statistical significance from unity using the one-sample *t*-test by first subtracting one from the ratio and comparing the result to zero. The Fisher exact test was used to compare the abundance of splice variants (fractions) between WKY and SHR in Figure 3A, whereas the $\chi^2$-test was used with the data in Figure 3C. Comparisons of all other data for WKY vs. SHR were made with the unpaired *t*-test or with the Mann–Whitney Rank Sum Test if data were identified as unsuitable for the *t*-test by SigmaPlot.

## RESULTS

### Basic animal characteristics

Systolic blood pressure measured by indirect tail cuff methods was significantly higher is SHR compared with WKY (Table 1). There were no significant differences in body weight while total heart weight and heart weight to body weight ratio were significantly higher in SHR (Table 1).

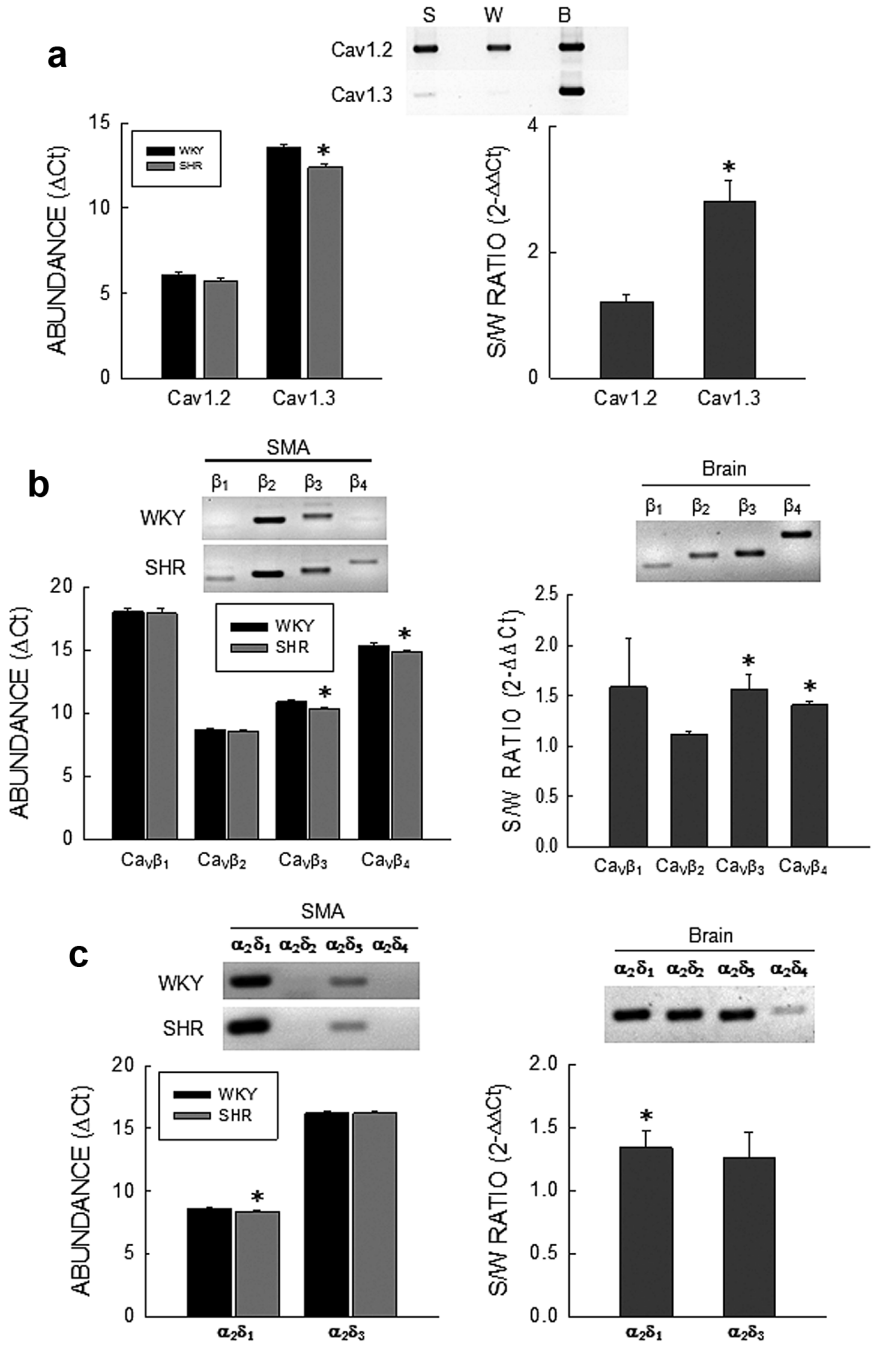


**Figure 1.** Gene expression of $Ca_V$ subunits in small mesenteric arteries (SMA). (**a**) $Ca_V$ $\alpha_1$ subunits. *Top*: EtBr stained gel of cPCR products from SHR (S), WKY (W), and brain (B). *Left*: Quantitative PCR results represented as $\Delta C_t$ values relative to β-actin. *Right*: Ratio of abundance of Cav1.2 and Cav1.3 in SHR to WKY represented as $2^{-\Delta\Delta C_t}$. $n = 9$ for both WKY and SHR. (**b**) $Ca_V$ β subunits. *Top*: EtBr stained gel of PCR products for $\beta_1$–$\beta_4$ subunits in SMA from SHR and WKY, and brain. *Left*: Quantitative PCR results represented as $\Delta C_t$ values relative to β-actin. *Right*: Ratio of abundance of $\beta_1$–$\beta_4$ in SHR to WKY represented as $2^{-\Delta\Delta C_t}$. $n = 4$ for both WKY and SHR. (**c**) $Ca_V$ $\alpha_2\delta$ subunits. *Top*: EtBr stained gel of PCR products for $\alpha_2\delta_1$–$\alpha_2\delta_4$ subunits in SMA from SHR and WKY, and brain. *Left*: Quantitative PCR results represented as $\Delta C_t$ values relative to β-actin. *Right*: Ratio of abundance of $\alpha_2\delta_1$ and $\alpha_2\delta_3$ in SHR to WKY represented as $2^{-\Delta\Delta C_t}$. $n = 4$ for both WKY and SHR. Bars and vertical lines represent the mean and 1 SEM, respectively. The star (*) indicates statistically significant differences between WKY and SHR for $\Delta C_t$ analysis ($P < 0.05$, unpaired *t*-test) and statistically significant differences from unity for $2^{-\Delta\Delta C_t}$ analysis ($P < 0.05$, one sample *t*-test).

### $Ca_V$ subunit expression

$Ca^{2+}$ currents recorded from SMA myocytes were previously shown to be completely inhibited by 10 μmol/l nifedipine suggesting the presence of only Cav1 $\alpha_1$-subunits.[6] cPCR showed high levels of Cav1.2 and trace levels of Cav1.3 expression in mRNA from WKY and SHR myocytes (Figure 1A, top). No expression of Cav1.1 or Cav1.4 was found. qPCR showed no significant differences in gene expression for Cav1.2 between WKY and SHR by $\Delta C_t$ (unpaired *t*-test) and $2^{-\Delta\Delta C_t}$ analysis (SHR/WKY = 1.18 ± 0.09; $n$ = 9, one sample *t*-test), whereas

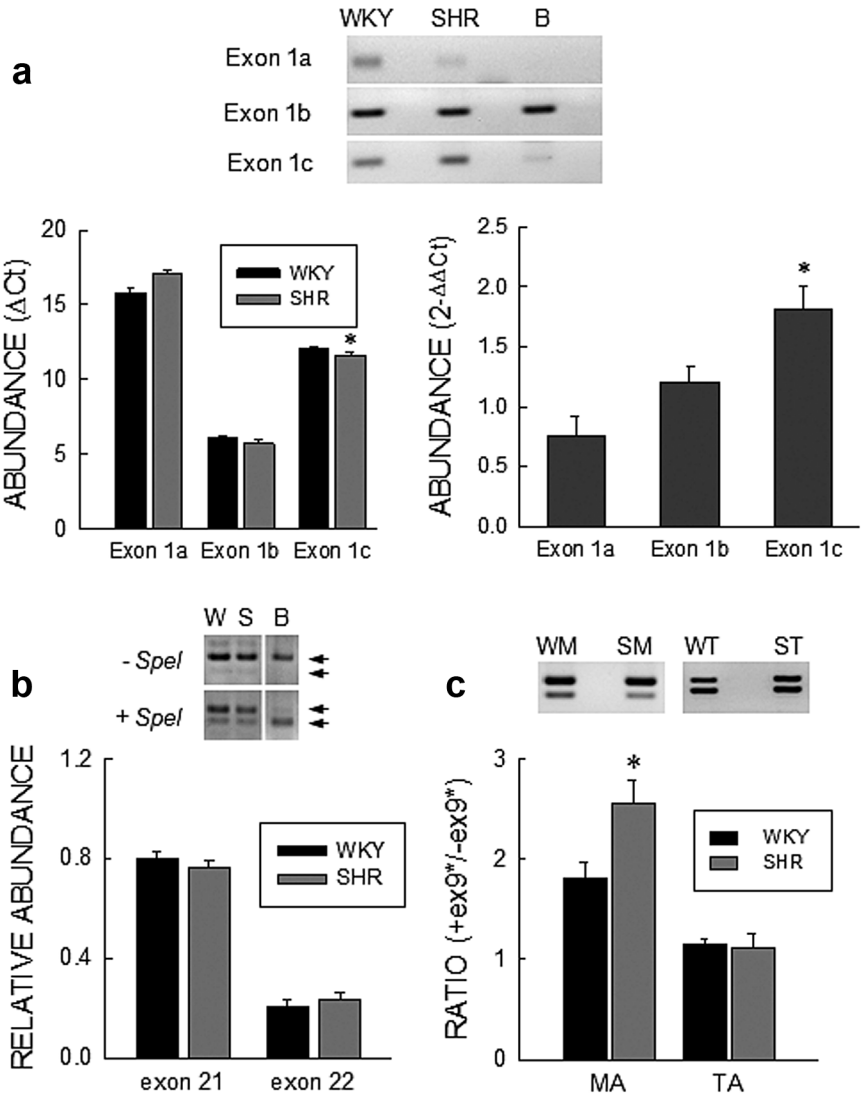


**Figure 2.** Expression of Cav1.2 splice variants. (**a**) Exon1 variants. *Top*: EtBr stained gel of PCR products for Cav1.2 exon1a, 1b, and 1c in SMA from SHR and WKY, and brain. (**b**) *Left*: Quantitative PCR results represented as $\Delta C_t$ values relative to β-actin. *Right*: Ratio of abundance of Cav1.2 exon1a, 1b, and 1c in SHR to WKY represented as $2^{-\Delta\Delta C_t}$. $n = 7$ for both WKY and SHR. (**b**) Exon21/22. *Top*: EtBr stained gels of PCR products spanning exons21 and 22 with or without treatment with *SpeI* for WKY (W) and SHR (S), and brain (B). *Bottom*: Densitometry analysis of gels for exon21 (*SpeI*-insensitive) and exon22 abundance (*SpeI*-sensitive minus null fraction); $n = 8$ for both WKY and SHR. (**c**) Exon 9*. *Top*: EtBr stained gel of PCR products for Cav1.2 spanning exon9* in SMA (M) and TA (T) from SHR and WKY. *Bottom*: Densitometry analysis of the ratio of +exon 9* to –exon9* transcript abundance in MA and TA from WKY (WM and WT) and SHR (SM and ST); $n = 8$ for WM, SM, WT, and ST. Bars and vertical lines represent the mean and 1 SEM, respectively. The star (*) indicates statistically different between WKY and SHR ($P < 0.05$). $\Delta C_t$ data in panel a and data in panel c were compared using the unpaired *t*-test, while values from the $2^{-\Delta\Delta C_t}$ analysis were compared by the one-sample *t*-Test.

gene expression of Cav1.3 was significantly higher in SHR by both $\Delta C_t$ and $2^{-\Delta\Delta C_t}$ analysis (SHR/WKY = 2.81 ± 0.33; $n = 9$, one sample *t*-test) (Figure 1A).

Using primers common to all splice variants of individual $Ca_V\beta$s, cPCR showed gene expression of all four β subunits in WKY and SHR mRNA with high levels of $\beta_2$ and $\beta_3$, low levels of $\beta_4$, and trace levels of $\beta_1$ (Figure 1B). This profile was significantly different from brain mRNA expression where cPCR showed expression of $Ca_V\beta$s in the following abundance order: $\beta_4 > \beta_3 > \beta_2 > \beta_1$. qPCR by both $\Delta C_t$ (unpaired *t*-test) and $2^{-\Delta\Delta C_t}$ analysis showed that the mRNA abundance of $\beta_3$ (1.56 ± 0.15; $n = 4$, one sample *t*-test) and $\beta_4$ (1.41 ± 0.04; $n = 4$, one sample *t*-test) were significantly higher in SHR but not $\beta_1$ or $\beta_2$ (Figure 1B).

cPCR showed gene expression of $\alpha_2\delta_1$ and $\alpha_2\delta_3$ at what appeared to be high and low levels, respectively, with no apparent expression of either $\alpha_2\delta_2$ or $\alpha_2\delta_4$ in either WKY or SHR mRNA (Figure 1C), which was significantly different from the brain expression profile. qPCR ($\Delta C_t$ and $2^{-\Delta\Delta C_t}$ analysis) confirmed this and showed that $\alpha_2\delta_1$ represented about 98% of the total in both WKY and SHR (Figure 1C). mRNA abundance of $\alpha_2\delta_1$ (1.34 ± 0.13; $n = 4$, one sample *t*-test) but not $\alpha_2\delta_3$ was significantly higher in SHR (Figure 1C).

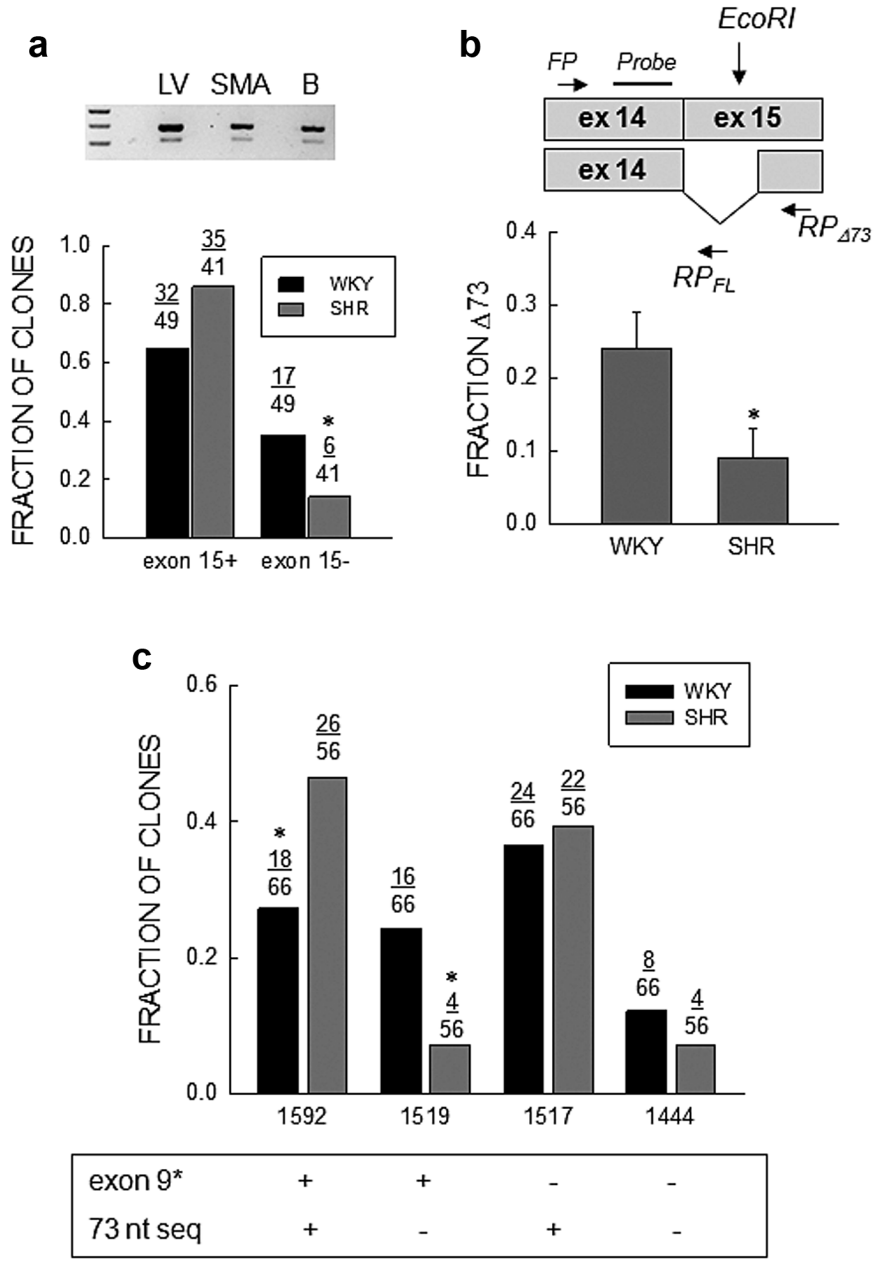


**Figure 3.** Abundance of Cav1.2Δ73 transcripts. (**a**) Fraction of clones. *Top*: EtBr stained gel of PCR products for Cav1.2 spanning exon15 from left ventricle, SMA, and brain. (**b**) *Bottom*: Fraction of full length (exon15+) or truncated (exon15−) clones relative to the total number in WKY ($n = 49$) and SHR ($n = 41$) SMA analyzed by sequencing. The star (*) indicates a statistically significant difference between WKY and SHR (Fisher exact test; $P = 0.05$). (**b**) Quantitative PCR. *Top*: Schematic representation of the location of the forward (FP) and reverse (RP) qPCR primers, and the probe for the 73 nucleotide (nt) deletion (Δ73) in exon15 plus full length transcripts with the location of the *EcoRI* site in exon15. *Bottom*: Analysis of abundance of the 73 nt deletion shown as the ratio of deleted to total Cav1.2 transcripts (Δ73/(Δ73 + FL)). Bars and vertical lines represent the mean and 1 SEM ($n = 7$), respectively, and star (*) indicates values statistically different from unity (unpaired *t*-test; $P < 0.05$). (**c**) Combinatorial analysis of expression of exons9* and exon15Δ73. The fraction of clones with and/or without exon9* and/or exon15Δ73 are shown for WKY and SHR. The "FL or +" indicate full length clones and the "−" clones with the 73 nt deletion. The star (*) indicates statistically significant difference between WKY and SHR ($\chi^2$-test; $P = 0.03$ for 1592 and $P = 0.01$ for 1519).

### $Ca_V$ $\alpha_1$ subunit splice variants

To determine splice variant gene expression profile in SMA, the entire open reading frame of Cav1.2 $\alpha_1$ was amplified by cPCR using multiple RNA preparations of both WKY and SHR. Assembled sequences from multiple clones (Sequencer v4.8, Gene Codes Corp., Ann Arbor, MI) showed the presence of four mutually exclusive and four alternative exons.

For the mutually exclusive exons, we found gene expression of all three exon1 variants in SMA mRNA (Figure 2A). However, qPCR ($\Delta C_t$) showed exon1b to be the most abundant with expression of exon1c at low and exon1a at trace levels (Figure 2A). The ratio of abundance of exon1b to exon1c

**Table 1.** General animal characteristics

| Group | *N* | BW (g) | HW (g) | HW/BW (mg/g) | SBP (mm Hg) |
|---|---|---|---|---|---|
| WKY | 21 | 418 ± 11 | 1.33 ± 0.04 | 3.17 ± 0.03 | 127 ± 4 |
| SHR | 21 | 422 ± 8 | 1.65 ± 0.04* | 3.91 ± 0.10* | 181 ± 4* |

Abbreviations: *n* = number of animals; BW = body weight in g; HW = heart weight in g; HW/BW = ratio of heart weight to body weight in mg/g; SBP = indirect systolic blood pressure in mm Hg;
*$P < 0.05$ (unpaired *t*-test).

was about 60:1, whereas the ratio of exon1b to exon1a was more than 1000:1 for both WKY and SHR. qPCR ($2^{-\Delta\Delta C_t}$ analysis) showed that mRNA abundance of exon1c (1.81 ± 0.19; $n = 7$, one sample *t*-test) but not exon1b (1.21 ± 0.12; $n = 7$ in one sample *t*-test) or exon1a (0.76 ± 0.16; $n = 7$ in one sample *t*-test) was significantly different between SHR and WKY (Figure 2A).

For exons8/8a, analysis of multiple clones showed that exon8 represented the majority of the total clones with no difference between WKY (94% ± 2%, $n = 8$) and SHR (93% ± 2%, $n = 8$). For exons21/22,[13] cPCR analysis showed a small fraction of transcripts to be null for both which was not different between WKY (4% ± 1%, $n = 8$) and SHR (3% ± 1%, $n = 8$). To distinguish between exon21 and 22, we took advantage of the presence of a *SpeI* restriction site in exon22. *SpeI* insensitive clones (exon21) analyzed by densitometry represented the majority with a similar abundance in WKY (80% ± 3%, $n = 8$) and SHR SMA (76% ± 3%, $n = 8$) (Figure 2B). For comparison, the majority of clones in brain contained exon22 (Figure 2B). Analysis of multiple clones for exons31/32, showed that exon31 was present in 100% of clones for both WKY and SHR.

Of the variable exons in Cav1.2 $\alpha_1$, the abundance of transcripts containing exon9* was significantly higher than those lacking it in both WKY ($n = 8$) and SHR ($n = 8$) SMA (Figure 2C) with a significantly larger ratio in SHR. A similar analysis using RNA from tail artery myocytes showed a lower abundance of exon9* containing transcripts compared to SMA with no significant difference between WKY ($n = 8$) and SHR ($n = 8$).

Sequencing cDNAs that included Domain II revealed clones with a 73 nt deletion at the proximal end of exon15 that were less frequent in SHR (Figure 3A). To quantitate the abundance of transcripts with and without the 73 nt deletion (exon15Δ73), we took advantage of an *EcoRI* restriction site within the 73 nt sequence (Figure 3B). We first amplified a fragment (205 nt) of Cav1.2 $\alpha_1$ that completely spanned exon15 with 10 cycles of cPCR. We then incubated 5 µl aliquots of this reaction with active or heat inactivated (15 minutes at 65 °C empirically determined) *EcoRI* at 37 °C for 2 hour in a reaction volume of 10 µl. We then took two 5 µl aliquot of each "digest" for two qPCR reactions with a common forward primer and probe, and two different reverse primers. One was located in exon15 upstream from the *EcoRI* site for full length transcripts ($RP_{FL}$) and the other in exon15 downstream from the alternative splice acceptor site used to splice out the 73 nt fragment ($RP\Delta_{73}$) for Δ73 transcripts (Supplementary Figure S2). Results of this analysis confirmed a lower mRNA level of Cav1.2Δ73 in SMA from SHR ($n = 7$) compared with WKY ($n = 7$) (Figure 3B).

PCR analysis showed that transcripts including exon33 predominated (about 90%) in both WKY (90.1 ± 1.5, $n = 8$) and SHR (89.4 ± 2.5, $n = 8$) with no significant difference between groups. Finally, PCR and sequencing indicated that exon45 was absent in 100% of clones from WKY ($n = 8$) and SHR ($n = 8$). Sequences from all reactions were aligned (Sequencher v4.8, Gene Codes Corp., Ann Arbor, MI) to produce a consensus sequence which was similar to one reported for cerebral artery (DQ538522) with the exception of exon1.

Alternative splicing of exons in Cav1.2 has been suggested to be coupled producing preferential exon combinations.[11] From the results described above, the Cav1.2 exons differentially expressed in WKY and SHR are between segments IS5 and IIS6.[11] This region was amplified by cPCR using RNA from multiple preparations and clones sequenced. Four contigs were found after alignment that were the result of the inclusion or exclusion of exon9* and the proximal 73 nt of exon15 (Figure 3C). Compared to WKY ($n = 66$ clones), there was a larger fraction of cDNA clones containing both exon9* and full-length exon15, and a smaller number of clones with exon15Δ73 with or without exon9* in SHR ($n = 56$ clones). No difference in the fraction of clones containing the 73 nt cassette but lacking exon9* was found between the two groups.

### $Ca_V$ accessory subunit splice variants

In addition to $\alpha_1$ subunits, β, and $\alpha_2\delta_1$ subunits are also alternatively spliced.[14,15] Using cPCR and sequencing we found gene expression of the a, b, c and e variants of $\beta_2$ in the brain, but only $\beta_{2c}$ (AF394941) was present in mRNA of both WKY and SHR (Supplementary Figure S3).

$\alpha_2\delta_1$ subunits have been shown to contain regions of alternative splicing in exon19 (15 nt) and exon24 (21 nt).[15] cPCR showed exon24 to be absent in both WKY and SHR while gene expression of transcripts with ($\alpha_2\delta_{1d}$) and without ($\alpha_2\delta_{1e}$) exon19 were present in mRNA from both WKY and SHR. The former appeared to be more abundant as it was present after fewer PCR cycles in both WKY and SHR (Supplementary Figure S3). qPCR primers to quantitate gene expression of these splice variants that met our quality control criteria could not be found due to the short length of exon 19.

### Protein expression

Two forms of functional Cav1.2 $\alpha_1$-subunit protein previously identified[16] were both expressed at higher levels

in SHR compared with WKY in blots probed with a II-III loop antibody but not with an exon1b antibody. The smaller molecular weight form was dominant in both (Figure 4A). The difference in antibodies likely reflects the differences in transcripts containing exon15Δ73 between WKY and SHR, which do not code for full length (loop II-III containing) protein. Expression of $Ca_V\beta_3$ but not $Ca_V\beta_2$ protein was significantly higher in SHR (Figure 4B). For $\alpha_2\delta_1$ subunits two distinct components were found one of which was glycosylated (Supplementary Figure S4) and represented 80% of total $\alpha_2\delta_1$ protein in both WKY and SHR. The fully glycosylated $\alpha_2\delta_1$ protein which likely reflects plasma membrane located subunits[15] was significantly higher in SHR (Figure 4C).

### Functional effects

To assess the functional significance of differences in $Ca_V$ mRNA and protein expression between WKY and SHR reported herein, we compared the properties of $Ca^{2+}$ currents from native SMA myocytes (Figure 5A, C, and E) with those of cells heterologously expressing $Ca_V$ subunits (Figure 5B,

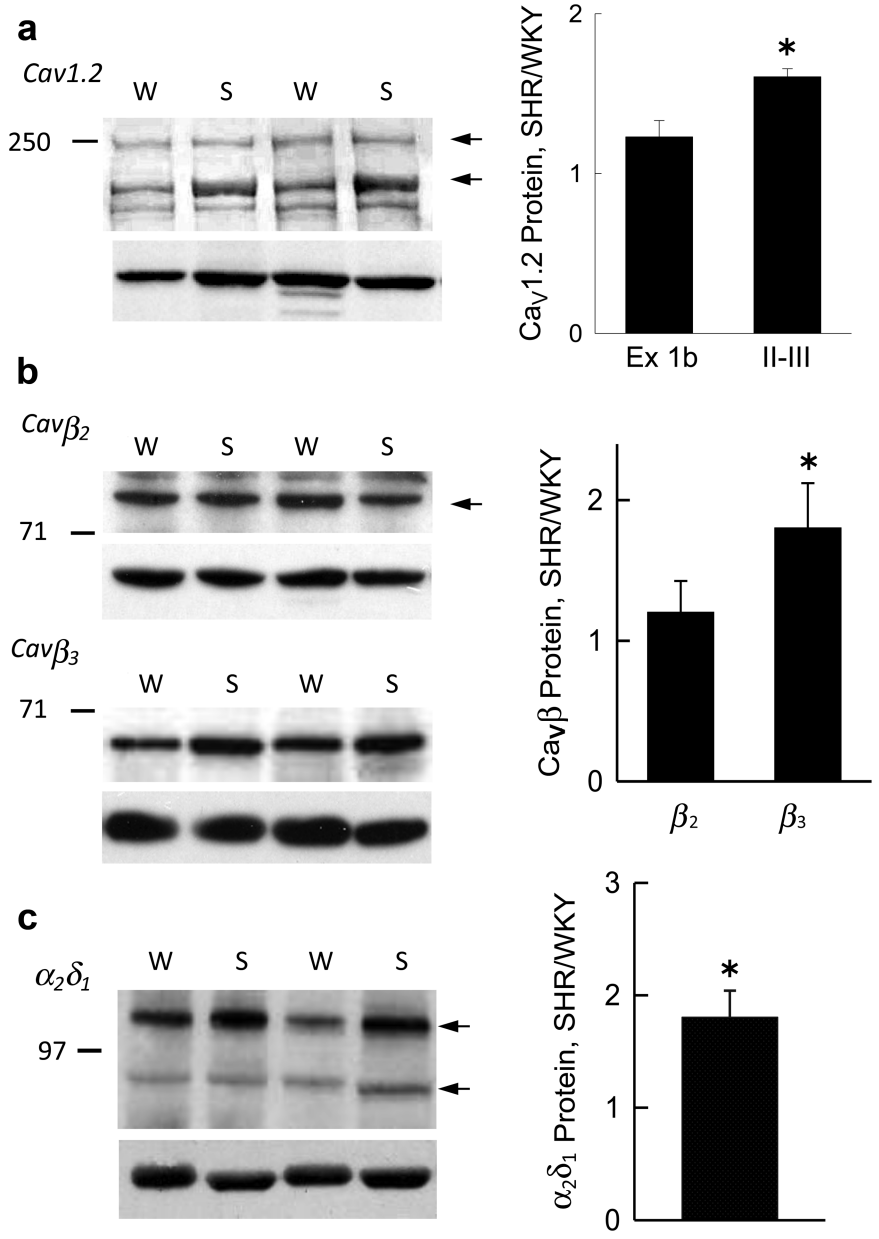


**Figure 4.** $Ca_V$ subunit protein expression. *Left*: Western blot of protein lysates from WKY (W) and SHR (S) probed with antibodies to (**a**) the II-III intracellular loop of Cav1.2 $\alpha_1$ (top) and β-actin (bottom); (**b**) $Ca_V\beta_2$ and $Ca_V\beta_3$ (top), and β-actin (bottom); and (**c**) $Ca_V\alpha_2\delta_1$ (top) and β-actin (bottom). *Right*: Graphs summarizing $Ca_V$ subunit protein expression determined by densitometry normalized to β-actin in SHR vs. WKY for (**A**) Cav1.2 $\alpha_1$ with exon1b ($n = 5$) and II-III loop ($n = 10$) antibodies; (**B**) $Ca_V\beta_2$ ($n = 8$) and $Ca_V\beta_3$ ($n = 8$), and (**c**) $Ca_V\alpha_2\delta_1$ ($n = 8$). Bars and vertical lines represent mean and 1 SEM, respectively, and star (*) indicates values statistically different from unity ($P < 0.05$, one sample *t*-test).

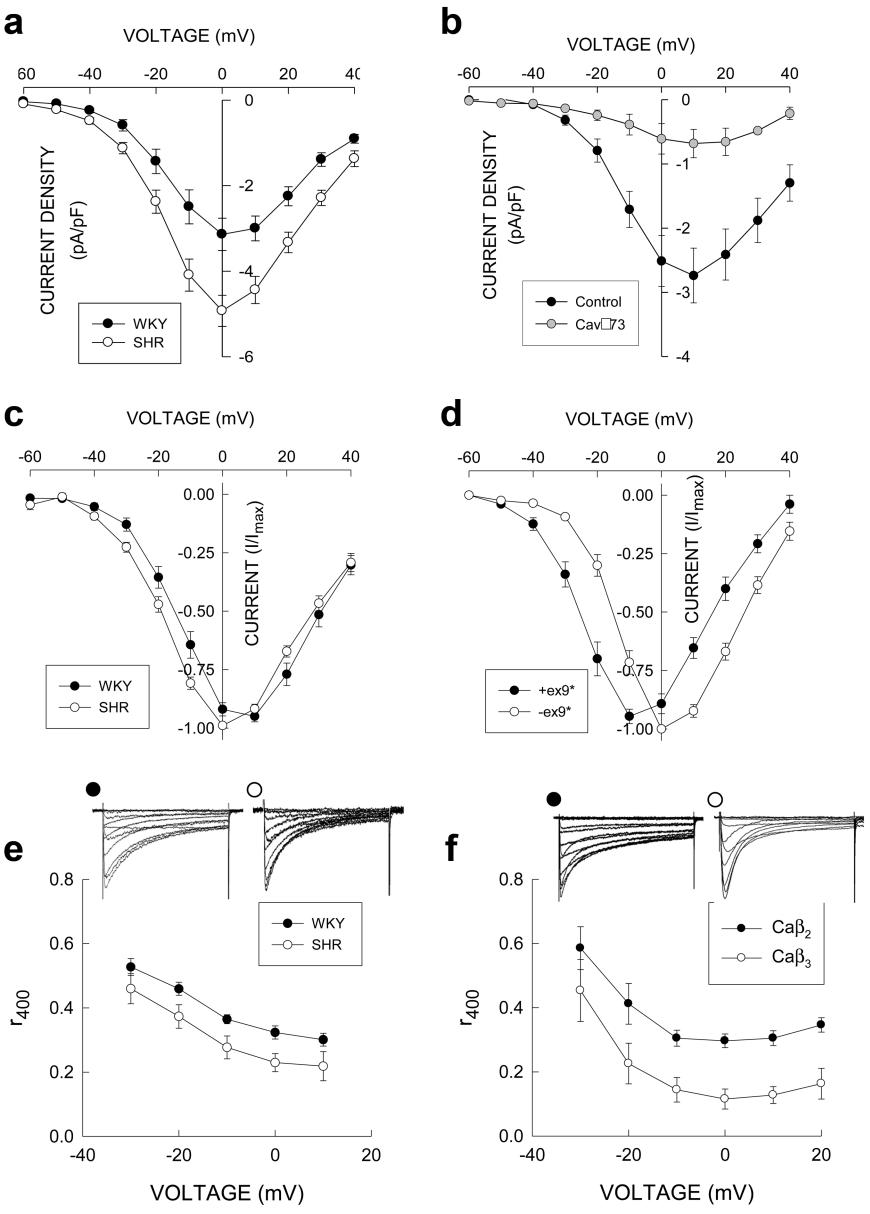


**Figure 5.** Functional effects of $Ca_V$ subunit differences. (**a**) $I_{Ca}$ (pA/pF) was larger in isolated SHR myocytes that have lower expression levels of Cav1.2Δ73 compared to WKY (data were replotted from Figure 3 in ref.[6] with permission). (**b**) Increasing expression of Cav1.2Δ73 decreased $I_{Ca}$ (pA/pF) in ASMC (data reproduced from Figure 5 in ref.[17]). (**c**) Voltage dependence of $I_{Ca}$ normalized to the maximum value is shifted in the negative voltage direction in SHR myocytes which have a higher level of expression of exon9* containing transcripts (data were replotted from ref.[6] with permission). (**d**) Voltage dependence of $I_{Ca}$ in HEK cells transfected with Cav1.2 constructs with (77–9*) or without (77-WT) exon9* (data were replotted from Figure 4 in ref.[18]). (**e**) $I_{Ca}$ inactivation represented as $r_{400}$ (current measured 400 milliseconds after the voltage clamp step divided by the peak value) was faster in SHR myocytes that have a higher level of $Ca_V\beta_3$ expression. (**f**) In transiently transfected HEK cells inactivation was faster (smaller $r_{400}$) in cells expressing $Ca_V\beta_3$ compared to $Ca_V\beta_{2c}$ along with the same Cav1.2 $\alpha_1$ and $\alpha_2\delta_1$ constructs. For (**e**) and (**f**), families of $Ca^{2+}$ currents recorded at voltages from −60 to +40 mV in 10 mV, 500-ms-long voltage steps from a holding potential of −80 mV are shown for each condition. For all panels, symbols and vertical lines represent the mean and ±1 SEM, respectively.

D, E and F). For this purpose, we used data previously published (Figure 5A–D) as well as newly analyzed (Figure 5E) and newly performed experiments (Figure 5F). In a previous study,[6] we found that peak $Ca^{2+}$ current density ($I_{Ca}$) was larger in SMA myocytes from SHR compared to WKY (Figure 5A). This difference is associated with higher protein levels of FL-Cav1.2 $\alpha_1$, $\beta_3$, and $\alpha_2\delta_1$ in SHR, and a lower abundance of transcripts coding for the truncated Cav1.2Δ73 vs. the full-length forms of Cav1.2 $\alpha_1$ reported herein. By comparison we previously reported that increasing expression of Cav1.2Δ73 in ASMC decreases $I_{Ca}$ (Figure 5B) demonstrating an inverse relation between Cav1.2Δ73 expression and peak $I_{Ca}$.[17]

In a previous publication, we reported that the voltage dependence of activation of $I_{Ca}$ in SHR myocytes (that have

a higher level of expression of exon9*) was shifted approximately −5 mV (Figure 5C) compared to WKY.[6] Based upon heterologous expression of $Ca_V$ subunits in HEK cells, Liao *et al.*[18] reported that the voltage dependence of activation of $Ca^{2+}$ channels containing Cav1.2 $\alpha_1$ subunits that included exon9* was shifted approximately −10 mV compared to $\alpha_1$ subunits lacking exon9* (Figure 5D).

This difference in voltage dependence of $I_{Ca}$ current–voltage curves between SHR and WKY produces a similar difference in the voltage dependence of conductance (Supplementary Figure S5A in supplementary results section). Combined with no difference in the voltage dependence of inactivation this difference shifts the voltage dependence of window currents to more negative voltages and increase its peak value (Supplementary Figure S5B in supplementary results section). When the differences in peak $Ca^{2+}$ current density between WKY and SHR are included an even larger difference exists in window currents especially in the physiological range of voltages (−60 to −30 mV).

In order to assess all inactivation processes[19] and to eliminate the subjectiveness of analyzing time constants of $I_{Ca}$ inactivation, the latter was represented as the ratio of $Ca^{2+}$ current 400 ms after the initiation of the voltage clamp step (to 0 mV from a holding potential of −80 mV) to the peak value (i.e., $r_{400}$). We applied this analysis to unpublished data from experiments previously performed in this laboratory and found that $I_{Ca}$ inactivation was faster (smaller $r_{400}$) in SHR myocytes (with higher levels of expression of $Ca_V\beta_3$) compared to WKY (Figure 5E). We transiently transfected HEK cells with $Ca_V\beta_{2c}$ ($n = 17$) or $Ca_V\beta_3$ ($n = 11$) plus Cav1.2 and $\alpha_2\delta_1$ and found that $Ca_V\beta_3$ conferred a faster inactivation (lower $r_{400}$) compared to $Ca_V\beta_{2c}$ (Figure 5F). Values of inactivation rate for $I_{Ca}$ at 0 mV in both WKY and SHR myocytes were intermediate between those of HEK cells expressing $Ca_V\beta_{2c}$ and $Ca_V\beta_3$ reflecting the expression of both subunits in native cells. Interestingly, we also found that conductance-voltage curves for $Ca^{2+}$ currents in HEK cells expressing $Ca_V\beta_3$ were shifted to the right compared to cells expressing $Ca_V\beta_{2c}$ (Supplementary Figure S6A). Combining these results with the differences in $Ca_V\beta$ protein expression between WKY and SHR predicts a small shift in the conductance-voltage curve to the right with a more prominent effect at negative voltages (Supplementary Figure S6B). Since this shift is opposite to that found in native myocytes, it must be concluded that the increase in exon9* containing $\alpha_1$ subunits in SHR is the primary mechanism responsible for the differences in voltage dependence of activation.

## DISCUSSION

Increased functional activity of $Ca_V$ in arteries[3,4] and larger $Ca^{2+}$ current density in isolated ASMC of hypertensive subjects is well documented.[6,20,21] We found greater Cav1.2 $\alpha_1$-protein without increased total mRNA in hypertensive arterial myocytes (HAM) in agreement with others,[21–23] and a lower abundance of Cav1.2 $\alpha_1$-transcripts containing exon15Δ73 (produced by alternative splicing[24]) that code for a truncated, nonfunctional subunit.[21] Thus, a larger fraction of total $\alpha_1$ transcripts code for full length protein in SHR (~90%) compared with WKY (~70%) which could contribute to larger Cav1.2 $\alpha_1$-subunit protein expression. Indeed, full length Cav1.2 $\alpha_1$ protein (II-III loop containing subunits) was found to be significantly larger in SHR. It is important to note that transcript abundance (total mRNA) and transcript diversity (splice variants) involve distinct processes that can be independently regulated,[25] and other factors such as mRNA and/or protein stability could also be involved in the enhanced Cav1.2 $\alpha_1$ protein expression in HAM.

Notably, both $Ca_V\beta_{3a}$ and $\alpha_2\delta_1$ were equivalently higher at both the transcript and protein level in SHR. Both $Ca_V\beta_3$[14] and $\alpha_2\delta_1$[15] subunits increase assembly of $Ca_V$ complexes enhancing trafficking to the plasma membrane, and β subunits decrease proteosomal degradation of $\alpha_1$ subunits[26] effectively increasing $\alpha_1$ protein half life. Also, both accessory subunits have been shown to be involved in the increased functional activity of $Ca_V$ in hypertensive ASMC.[20,21] The finding that protein expression of all three $Ca_V$ subunits is higher in hypertensive SMA is consistent with the suggestion that cell surface expression of $\alpha_1/\beta/\alpha_2\delta$ channel complexes may be regulated by cotranslation and ER assembly mechanisms.[27]

Heterologous expression studies have shown that expression of $Ca_V\beta_3$ with $\alpha_1$ and $\alpha_2\delta_1$ subunits produces a faster rate of inactivation of $Ca^{2+}$ currents compared to expression with $Ca_V\beta_2$, whereas coexpression of a mixture of $Ca_V\beta_2$ and $Ca_V\beta_3$ produces an intermediate rate of inactivation.[28] These findings were confirmed in this study. In addition, the rate of inactivation of $Ca_V$ in mice following $Ca_V\beta_3$ deletion is slower than wild type mice.[28] This suggests that the higher level of $Ca_V\beta_3$ protein in SHR is likely responsible for the faster rate of $Ca_V$ current inactivation in SHR.[7] It should be noted that differences do exist in the voltage dependence of $r_{400}$ between native myocytes (Figure 5E) and transfected HEK cells (Figure 5F). This is likely due to differences in other inactivating currents such as $Ca^{2+}$ sensitive $Cl^-$ currents between the cell types. Notably, at 0 mV where $Cl^-$ currents are expected to negligible due to the symmetrical $Cl^-$ conditions of the patch clamp experiments there is a close correspondence with the expected results. It is also interesting that protein expression of $Ca_V\beta_2$ is not different between WKY and SHR and is also not altered with $Ca_V\beta_3$ deletion in the mouse.[28] This suggests that regulation of $Ca_V\beta_3$ protein expression is independent of $Ca_V\beta_2$ and linked to blood pressure in some manner, and that $Ca_V\beta_2$ and $Ca_V\beta_3$ protein expression are not reciprocally regulated.[28]

Along with a smaller abundance of Cav1.2 $\alpha_1$ subunit transcripts with exon15Δ73, we found a larger abundance of exon9* in SHR myocytes. Furthermore, combinatorial analysis (Figure 3C) showed that the fraction of exon9* transcripts that also contained exon15Δ73 (−/+) was larger in WKY (24%) than in SHR (7%). Since exon15Δ73 containing transcripts are translated into a protein truncated in the IIS6 region and shown to be nonfunctional,[17] about 47% of exon9* containing transcripts in WKY are predicted not to code for functional channels compared to only 13% in SHR. Inclusion of exon9* in 100% of the channels in heterologously transfected cells produces a −10 mV shift in the voltage dependence of activation in exon1b containing Cav1.2 channels.[18] The difference in the $V_{0.5}$ of $I_{Ca}$ conductance

between WKY and SHR[6] is expected to be smaller than this value as less than 100% of the channels contain exon9*.

Although the general pattern of exon use found in SMA of both WKY and SHR was similar to most previous studies,[12] one interesting difference that did exist was in exon1.[12] Of the three transcript variants of exon1, exon1a is highly expressed in cardiac myocytes.[11] Of the other two, transcripts containing the newly identified exon1c predominate in cerebral arteries[12] while those with exon1b predominate in SMA. These findings support the concept of regional regulation of $Ca_V$ mRNA alternative splicing, and expression.

The lower levels and lack of a difference in exon9* abundance between WKY and SHR in RNA derived from TA myocytes compared to SMA is of interest. The TA is primarily involved in temperature regulation in the rat and in a normal laboratory environment the tail vasculature is relatively vasoconstricted which would be expected to lower transmural pressure in that area. This finding suggests that local factors not circulating blood borne agents are involved in this difference. It could be speculated that the lower abundance of exon9* in TA myocytes is related to the lower arterial pressure in the tail vasculature. Alternatively, the TA is highly innervated with neurotransmitters possibly playing a role in regulating the abundance of exon9*. This suggests that blood pressure or sympathetic nerve activity or their surrogates could be part of a signaling pathway that regulates exon9* inclusion.[29]

Two lines of evidence suggest that the differences in $Ca_V$ gene and protein expression reported herein are related to blood pressure rather than being differences between two genetically distinct animal groups. First, we showed that systolic blood pressure and peak $Ca_V$ current density (pA/pF) in SMA from both WKY and SHR determined in animals of different ages (6, 12, and 20 months) fall on the same linear regression curve.[6] Furthermore, chronic treatment of both WKY and SHR with ramipril decreases both systolic blood pressure and $Ca_V$ current density to points on the same curve.[30] This suggests that a deterministic relation exists between blood pressure and $Ca_V$ current in WKY and SHR SMA. Second, experimental hypertension produced by abdominal aorta constriction between the origins of the renal arteries produced an increase in Cav1.2 $\alpha_1$-subunit protein and $Ca^{2+}$ current but not mRNA (gene) expression in the "hypertensive" compared with the "normotensive" renal artery.[31] Also, experimental hypertension produced by angiotensin II infusion produced an increase in $Ca_V\beta_3$ protein expression and peak $Ca^{2+}$ current.[21] Thus, in models of experimental hypertension similar changes in $Ca_V$ subunit gene and protein expression and peak $Ca_V$ currents occur as in the SHR. Together, these results suggest that the differences in $Ca_V$ subunit gene and protein expression including splice variants reported herein represent an effect related to blood pressure or some surrogate as previously suggested[21,31] but cannot exclude a contribution from genetic differences.

## SUMMARY

The increased functional activity of $Ca_V$ in HAM is associated with increased $Ca^{2+}$ currents with altered gating and kinetics.[6,7] The former is associated with an increased number of $Ca_V$ channels, and the latter suggests differences in the molecular composition of $Ca_V$ complexes. This study reports for the first time a detailed study of gene and protein expression of $Ca_V$ subunits and their splice variants in SMA myocytes of mature SHR and WKY. The lower abundance of exon15Δ73 containing Cav1.2 transcripts plus the higher abundance of $Cav\beta_3$ and $\alpha_2\delta_1$ protein likely contribute to the greater functional activity of Cav1.2 channels in SHR. In SHR, the higher abundance of exon9* in full length Cav1.2 transcripts likely contributes to the difference in voltage dependence of $Ca_V$ activation, and the higher expression of $Ca_V\beta_3$ protein to the faster current inactivation. Finally, since Cav1.2Δ73 is produced by alternative splicing[24] and alternative splicing is a regulated process,[25] it is possible that the mechanisms that regulate the production of Cav1.2Δ73 are themselves regulated.[32] It is speculated that such processes could act to fine tune expression of Cav1.2 $\alpha_1$ protein in arterial myocytes.[33] Further studies are required to test this hypothesis, to determine the mechanisms involved in this process, and to determine their significance.

## SUPPLEMENTARY MATERIALS

Supplementary materials are available at *American Journal of Hypertension* (http://ajh.oxfordjournals.org).

## FUNDING

This work was supported by National Institutes of Health grant HL28476 (to R.H.C), American Heart Association grant 0350084N (to R.H.C.), and W. W. Smith Charitable Trust grant H0604 (to R.H.C.).

## DISCLOSURE

The authors declared no conflict of interest.

## REFERENCES

1. Sonoyama K, Greenstein A, Price A, Khavandi K, Heagerty T. Vascular remodeling: implications for small artery function and target organ damage. *Ther Adv Cardiovasc Dis* 2007; 1:129–137.
2. Drazner MH. The progression of hypertensive heart disease. *Circulation* 2011; 123:327–334.
3. Cox RH, Rusch NJ. New expression profiles of voltage-gated ion channels in arteries exposed to high blood pressure. *Microcirculation* 2002; 9:243–257.
4. Matsuda K, Lozinskaya I, Cox RH. Augmented contributions of voltage-gated Ca2+ channels to contractile responses in spontaneously hypertensive rat mesenteric arteries. *Am J Hypertens* 1997; 10:1231–1239.
5. Stekiel WJ. Electrophysiological mechanisms of force development by vascular smooth muscle in hypertension. In RMKW Lee (ed), *Blood Vessel Changes in Hypertension: Structure and Function*, Vol 2. CRC Press, Inc.: Boca Raton, FL, 1989, pp. 127–170.
6. Lozinskaya IM, Cox RH. Effects of age on Ca2+ currents in small mesenteric artery myocytes from Wistar-Kyoto and spontaneously hypertensive rats. *Hypertension* 1997; 29:1329–1336.
7. Cox RH, Lozinskaya IM. Ca2+ channel inactivation in small mesenteric arteries of WKY and SHR. *Am J Hypertens* 2008; 21:406–412.

8. Varadi G, Mori Y, Mikala G, Schwartz A. Molecular determinants of Ca2+ channel function and drug action. *Trends Pharmacol Sci* 1995; 16:43–49.
9. Cox RH, Fromme SJ, Folander KL, Swanson RJ. Voltage gated K+ channel expression in arteries of Wistar-Kyoto and spontaneously hypertensive rats. *Am J Hypertens* 2008; 21:213–218.
10. Cox RH, Folander K, Swanson R. Differential expression of voltage-gated K(+) channel genes in arteries from spontaneously hypertensive and Wistar-Kyoto rats. *Hypertension* 2001; 37:1315–1322.
11. Tang ZZ, Hong X, Wang J, Soong TW. Signature combinatorial splicing profiles of rat cardiac- and smooth-muscle Cav1.2 channels with distinct biophysical properties. *Cell Calcium* 2007; 41:417–428.
12. Cheng X, Liu J, Asuncion-Chin M, Blaskova E, Bannister JP, Dopico AM, Jaggar JH. A novel Ca(V)1.2 N terminus expressed in smooth muscle cells of resistance size arteries modifies channel regulation by auxiliary subunits. *J Biol Chem* 2007; 282:29211–29221.
13. Soldatov NM, Bouron A, Reuter H. Different voltage-dependent inhibition by dihydropyridines of human Ca2+ channel splice variants. *J Biol Chem* 1995; 270:10540–10543.
14. Birnbaumer L, Qin N, Olcese R, Tareilus E, Platano D, Costantin J, Stefani E. Structures and functions of calcium channel beta subunits. *J Bioenerg Biomembr* 1998; 30:357–375.
15. Klugbauer N, Marais E, Hofmann F. Calcium channel alpha2delta subunits: differential expression, function, and drug binding. *J Bioenerg Biomembr* 2003; 35:639–647.
16. Gerhardstein BL, Gao T, Bünemann M, Puri TS, Adair A, Ma H, Hosey MM. Proteolytic processing of the C terminus of the alpha(1C) subunit of L-type calcium channels and the role of a proline-rich domain in membrane tethering of proteolytic fragments. *J Biol Chem* 2000; 275:8556–8563.
17. Cox RH, Fromme SJ. A naturally occurring truncated Cav1.2 α1-subunit inhibits Ca2+ current in A7r5 cells. *Am J Physiol Cell Physiol* 2013; 305:C896–C905.
18. Liao P, Yu D, Lu S, Tang Z, Liang MC, Zeng S, Lin W, Soong TW. Smooth muscle-selective alternatively spliced exon generates functional variation in Cav1.2 calcium channels. *J Biol Chem* 2004; 279:50329–50335.
19. Cens T, Restituito S, Galas S, Charnet P. Voltage and calcium use the same molecular determinants to inactivate calcium channels. *J Biol Chem* 1999; 274:5483–5490.
20. Bannister JP, Bulley S, Narayanan D, Thomas-Gatewood C, Luzny P, Pachuau J, Jaggar JH. Transcriptional upregulation of α2δ-1 elevates arterial smooth muscle cell voltage-dependent Ca2+ channel surface expression and cerebrovascular constriction in genetic hypertension. *Hypertension* 2012; 60:1006–1015.
21. Kharade SV, Sonkusare SK, Srivastava AK, Thakali KM, Fletcher TW, Rhee SW, Rusch NJ. The β3 subunit contributes to vascular calcium channel upregulation and hypertension in angiotensin II-infused C57BL/6 mice. *Hypertension* 2013; 61:137–142.
22. Pratt PF, Bonnet S, Ludwig LM, Bonnet P, Rusch NJ. Upregulation of L-type Ca2+ channels in mesenteric and skeletal arteries of SHR. *Hypertension* 2002; 40:214–219.
23. Wang WZ, Saada N, Dai B, Pang L, Palade P. Vascular-specific increase in exon 1B-encoded CAV1.2 channels in spontaneously hypertensive rats. *Am J Hypertens* 2006; 19:823–831.
24. Soldatov NM. Genomic structure of human L-type Ca2+ channel. *Genomics* 1994; 22:77–87.
25. Moore MJ, Silver PA. Global analysis of mRNA splicing. *RNA* 2008; 14:197–203.
26. Li Q, Sarna SK. Chronic stress targets posttranscriptional mechanisms to rapidly upregulate α1C-subunit of Cav1.2b calcium channels in colonic smooth muscle cells. *Am J Physiol Gastrointest Liver Physiol* 2011; 300:G154–G163.
27. Brust PF, Simerson S, McCue AF, Deal CR, Schoonmaker S, Williams ME, Veliçelebi G, Johnson EC, Harpold MM, Ellis SB. Human neuronal voltage-dependent calcium channels: studies on subunit structure and role in channel assembly. *Neuropharmacology* 1993; 32:1089–1102.
28. Murakami M, Yamamura H, Suzuki T, Kang MG, Ohya S, Murakami A, Miyoshi I, Sasano H, Muraki K, Hano T, Kasai N, Nakayama S, Campbell KP, Flockerzi V, Imaizumi Y, Yanagisawa T, Iijima T. Modified cardiovascular L-type channels in mice lacking the voltage-dependent Ca2+ channel beta3 subunit. *J Biol Chem* 2003; 278:43261–43267.
29. Tang ZZ, Zheng S, Nikolic J, Black DL. Developmental control of CaV1.2 L-type calcium channel splicing by Fox proteins. *Mol Cell Biol* 2009; 29:4757–4765.
30. Cox RH, Lozinskaya I, Matsuda K, Dietz NJ. Ramipril treatment alters Ca(2+) and K(+) channels in small mesenteric arteries from Wistar-Kyoto and spontaneously hypertensive rats. *Am J Hypertens* 2002; 15:879–890.
31. Pesic A, Madden JA, Pesic M, Rusch NJ. High blood pressure upregulates arterial L-type Ca2+ channels: is membrane depolarization the signal? *Circ Res* 2004; 94:e97–e104.
32. Chen M, Manley JL. Mechanisms of alternative splicing regulation: insights from molecular and genomics approaches. *Nat Rev Mol Cell Biol* 2009; 10:741–754.
33. Chiu YH, Alvarez-Baron C, Kim EY, Dryer SE. Dominant-negative regulation of cell surface expression by a pentapeptide motif at the extreme COOH terminus of an Slo1 calcium-activated potassium channel splice variant. *Mol Pharmacol* 2010; 77:497–507.